



Catalytic Performance and Stability of Fe-Doped CeO₂ in Propane Oxidative Dehydrogenation Using Carbon Dioxide as Oxidant

Journal:	<i>Catalysis Science & Technology</i>
Manuscript ID	CY-ART-03-2020-000586.R1
Article Type:	Paper
Date Submitted by the Author:	11-May-2020
Complete List of Authors:	Wang, Hedun; Rutgers University Department of Chemical and Biochemical Engineering Tsilomelekis, George; Rutgers University Department of Chemical and Biochemical Engineering

Catalytic Performance and Stability of Fe-Doped CeO₂ in Propane Oxidative Dehydrogenation Using Carbon Dioxide as Oxidant

Hedun Wang^a and George Tsilomelekis*^a

Received 00th January 20xx,
Accepted 00th January 20xx

DOI: 10.1039/x0xx00000x

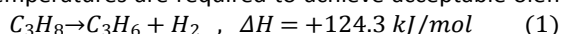
Propane oxidative dehydrogenation (ODH) in the presence of CO₂ was investigated over a series of Fe-doped CeO₂ catalysts. The well-recognized properties of cerium oxide materials regarding improved oxygen mobility and oxygen storage capacity (OSC) was utilized towards the synthesis of stable catalytic systems. The iron-cerium oxide solid solution catalysts with Fe dopant content from 1% up to 15% were successfully synthesized via co-precipitation method and calcined at 873K. It was confirmed by XRD and Raman characterization that all samples featured single cerianite crystalline phase with periodic lattice Ce ions substituted by Fe ions, with no hematite phase identified. Initial screening of catalytic behavior showed that propane ODH pathway was enhanced at high Fe/Ce ratio while propane cracking was suppressed. Stable propane conversion and propylene selectivity for up to 20 hours was achieved for the synthesized catalysts with moderate Fe loading. Ex-situ Raman, XPS and STEM was applied to analyze post-reaction catalyst and confirmed that deactivation occurred over low Fe catalysts were resulted from coke deposition on the surface, while CeO₂ sintering and Fe migration to form nanocrystals were the primary deactivation reasons for high Fe loading catalysts.

Key words: propane oxidative dehydrogenation; Fe-CeO₂ solid solution; surface oxygen vacancy; stability; deactivation

Introduction

Propylene is undoubtedly among the most important and fastest growing in demand petrochemicals. Although fluid catalytic cracking (FCC) as well as steam cracking processes are still widely utilized, research efforts have been placed in developing new technologies that maximize propylene production while addressing the big gap between supply and demand. Vast availability of low molecular weight alkanes due to the recent shale gas revolution is considered as a game-changing opportunity towards the potential development of 'on-purpose' production processes. Propane direct dehydrogenation (DH) as well as oxidative dehydrogenation (ODH) have attracted worldwide academic and industrial interests, but both suffer from limitations that have been reviewed extensively elsewhere¹⁻³.

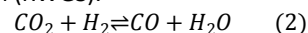
Propane DH is an endothermic reaction and thus high temperatures are required to achieve acceptable olefin yields.



The CATOFIN[®] dehydrogenation process⁴⁻⁵ provides 850000 MTA (million metric tons annually) of propylene with minimum of 99.5% purity and is based on chromium oxide supported on activated alumina. The toxicity of the chromium-based catalysts, especially the hexavalent chromium species that initially dominate the surface of the catalyst, is an important issue. The Oleflex dehydrogenation process⁴⁻⁵ relies on the traditional Pt/Sn catalytic system to produce polymer grade propylene. The high operating temperature as well as the cost of the Pt catalysts comprise the main drawbacks. In addition, the reaction is usually accompanied by catalyst deactivation due to coke formation and spatial separation of Pt-Sn species thus highlighting the stability of catalysts used among the major bottlenecks⁶⁻⁷.

On the other hand, although the exothermic character of propane ODH with O₂ has the potential to significantly reduce the reaction temperature, the fate of the desired propylene is difficult to be controlled due to unavoidable combustion of propane as well as of propylene to carbon monoxide and/or dioxide thus significantly lowering propylene selectivity. Even though there is very rich literature on various catalytic systems (e.g. metals, transition metal oxides, rare-earth metal oxides, metal carbides, supported alkali oxides and supported alkali chlorides), the lack of suitable catalysts that exhibit high activity while maintaining promising olefin selectivity is hampering potential endeavors for large scale commercializing.

The aforementioned competitive reaction network due to the overoxidation of paraffins and/or olefins can be suppressed by replacing oxygen with a weak oxidant, such as carbon dioxide⁸. The use of CO₂ as, alternative to oxygen, soft oxidant has the potential to i) avoid deep oxidation of alkanes/alkenes, ii) reduce coke formation and iii) favor propane conversion due to participation of the produced hydrogen in the reverse water-gas shift reaction (RWGS).



In recent years, a large variety of metal oxide catalysts have been explored in propane ODH with CO₂ with dispersed chromium oxide species to show great potential as active sites towards high conversion and selectivity. XANES and XPS results for spent catalysts have shown that during the reaction process⁹⁻¹¹, Cr⁶⁺ undergoes a rapid reduction to Cr³⁺/Cr²⁺, which is crucial for catalytic activity¹²⁻¹⁶. With CO₂ being a soft oxidant, it was found that reduced Cr species can be partially re-oxidized to higher oxidative states. Although promising initial propylene yield was achieved, Cr-based catalysts suffer from severe and rapid deactivation within a short time, regardless of sample preparation, reaction conditions and reactor design. The proposed reasons behind the severe deactivation encompassing potential coking^{11, 13, 17-18}, collapse of catalyst mesoporous structure¹⁷, agglomeration of reduced Cr to Cr₂O₃¹⁹, etc. In addition, Zhang et al. have suggested the

^a Department of Chemical and Biomolecular Engineering, Rutgers, The State University of New Jersey. Email: gt241@soe.rutgers.edu
Electronic Supplementary Information (ESI) available: See DOI: 10.1039/x0xx00000x

reduction of Cr(VI) to Cr(III)/Cr(II) as the main reason behind deactivation²⁰.

Pioneering work by the research group of JG Chen has provided molecular level understanding on light alkane CO₂ assisted ODH over non-precious metal (Fe-Ni) and precious metal (Fe-Pt, Ni-Pt) over CeO₂²¹⁻²⁶. Recently, the effect of oxide supports was also investigated by the same research group highlighting the CeO₂ as the most promising support²⁶ due to its ability to activate CO₂ via direct C=O bond scission. Olefin selectivity was found to depend on competitive reaction pathways such as ODH, reverse water gas shift as well as alkane dry reforming that can be tuned via rational selection of the bimetallic composition of active sites. DFT calculations suggested that Fe-Ni surface favors C-H bond scissoring while Pt-determined surface favors C-C cleavage. Additional evidence from EDS and TGA of spent Fe-Ni catalyst deactivation showed small regions of higher Fe content as compared to fresh catalyst thus excluding coking as the main deactivation reason.

In this work, we report a series of Fe doped CeO₂ as catalysts that show enhanced stability and promising catalytic performance for the propane oxidative dehydrogenation using CO₂ as soft oxidant. The well-reported oxygen mobility and oxygen storage capacity (OSC) of ceria based catalysts sets the foundation and main hypothesis of this work towards the formation of stable surface active sites²⁷⁻²⁸. To that end, we introduce Fe³⁺, which is proved to be active for propane dehydrogenation^{23, 29-30} as well as CO₂ activation^{21, 23, 31}, into ceria lattice with a series of Fe/Ce molar ratios.

Experimental

Materials and synthesis of catalysts

Ce(NO₃)₃·6H₂O (99.99%) and Fe(NO₃)₃·9H₂O (99.95%) were purchased from Sigma Aldrich and used without further purification. A series of Fe-doped ceria materials as bimetallic oxide catalyst (xFeCeO₂T, x indicates the molar percentage of Fe over Ce atoms; T indicates the calcination temperature in degree Celsius) were prepared batchwise via a co-precipitation method, as reported elsewhere³²⁻³⁴. In a typical synthesis, pre-calculated amount of precursor solutions was mixed and heated up to 343K under stirring. NH₄OH (Sigma Aldrich 30%) was added dropwise as precipitating agent by elevating solution pH value. Mixed precursor solution was kept stirring for 1 hour when pH adjusted around 7-8. Additional ammonium solution was added dropwise until pH reached 10.5. The mixture was kept at 343K for 24 hours. The precipitation mixture was then filtered, washed thoroughly with 1L DI water and 200ml pure ethanol, and then dried at 110°C overnight.

Determination of calcination temperature

Calcination temperature is crucial for phase transformation and crystalline growth, as well as removal of surface hydroxyl groups and possible carbon-based organics. Fe-doped ceria from the same synthesis batch were calcined at different temperatures and characterized by BET, Raman and XRD. As shown in the Supporting Information, (Figures S1, Table S1) calcination at 600°C is beneficial in the following aspects: higher

specific surface area and formation of Fe-Ce solid solution rather than two separated cerianite-hematite phases is achieved. Although it has been shown in the open literature that 450°C is a suitable temperature in terms of formation of Fe-Ce solid solution structure³⁵, the actual reaction conditions (as shown later) for CO₂ assisted propane ODH require higher temperature (550-600°C) and as a consequence, all samples studied for catalytic tests were calcined at 600°C as an optimal temperature.

Characterization methods

All prepared samples were thoroughly characterized prior the catalytic performance tests in order to obtain their physicochemical properties.

BET analysis

BET surface area measurements were conducted with Micromeritics TriStar 3000 (Serial # 2111) system. Typically, around 30mg of catalyst was loaded into a BET tube and degassed at 150°C for 8 hours prior to BET analysis in order to completely remove chemisorbed water from sample surface. Thirteen points were collected within 0.05 to 0.3 P/P₀ with 0.02 increment.

X-ray Powder Diffraction (XRD)

XRD analysis was performed with a PANalytical Philips X'Pert X-Ray diffractometer to determine crystallinity and phase composition. The XRD instrument is equipped with a CuKα source at 40 kV and 40 mA and angular incidence 2θ between 20° and 90° with 0.05° step and 4.0 s/step. The phase composition was analysed by whole pattern fitting (WPF) refinement 2-phase analysis with relative error R% targeted below 15%. Silicon was used as an external standard reference to determine any possible peak shift.

Raman spectroscopy

Raman spectra of the samples were collected with a Horiba Scientific LabSpec HR Evolution Raman spectrometer cooled with a Synapse CCD detector (-70°C). The laser line used (532nm solid-state, 80mw) was directed on the sample and focused by using a 50X long working distance objective. The power of the laser was kept at a low value to avoid overheating by using a neutral density filter (5%). The acquisition time was 30 seconds with a total of twenty accumulations.

X-ray photoelectron Spectroscopy (XPS)

X-ray Photoelectron Spectroscopy analysis were performed with 180° double focusing hemispherical analyzer and Al-Kα X-ray monochromatic source (400mm analysis spot size). The post-reaction catalysts were sieved with 325 mesh. All samples were exposed to air in a sufficient long time before analysis.

Scanning Transmission Electron Microscopy (STEM)

Both the imaging and electron energy loss (EEL) data were acquired by a Nion UltraSTEMTM 100. The microscope was operated at 60 kV with a probe convergence semi-angle of 35 mrad and an energy loss collection semi-angle of 34 mrad. The EEL spectrum image (SI) data was processed using Hyperspy1, a python-based microscopy analysis package. After background removal, the intensity of each element in the SI data was normalized to its maximum value in the SI map such that one can visualize the spatial distribution of the elements in the acquired area.

Catalytic performance test

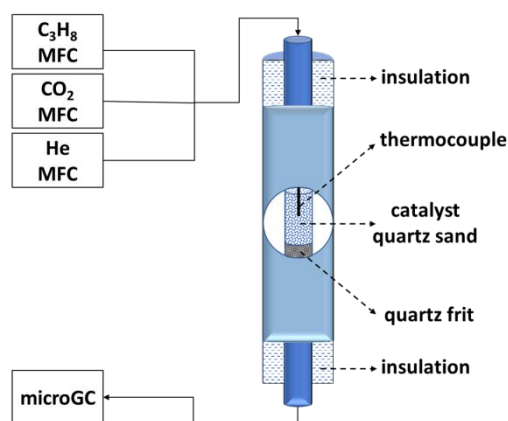
The catalytic activity was evaluated in a fixed bed quartz tube reactor (4mm ID) packed with 200mg catalyst diluted in 1000 mg of quartz sand (ACROS Organics 40-100 mesh). Reactants co-feed consists of propane (Airgas, 50% in nitrogen), CO₂ (Airgas, BD) and N₂ (Airgas, UHP). The reactant mixture was fed into the reactor (Scheme 1) with a flowrate varying from 10 to 30mL/min with 5% propane and 5% carbon dioxide in balancing nitrogen, unless otherwise stated. The catalyst was preheated in oxygen (Airgas, UHP) with 5K/min until the desired reaction temperature and kept in the same gas environment for 30mins to ensure the presence of fully oxidized catalyst. The catalysts were evaluated for the ODH reaction in the temperature range of 450 to 600°C and atmospheric pressure. The outlet stream was analysed with an in-line microGC (Agilent 490) equipped with MS5A column (for CH₄, CO and H₂) and PoraPlot Q column (for CO₂, C₂H₄, C₂H₆, C₃H₆, C₃H₈). Calculations of reactant conversion, selectivity and yield to main product and by-products were estimated as follow:

$$X_{C_3H_8} = \frac{F_{in, C_3H_8} - F_{out, C_3H_8}}{F_{in, C_3H_8}} \times 100\%$$

$$S_{C_3H_6} = \frac{F_{C_3H_6}}{F_{in, C_3H_8} - F_{out, C_3H_8}} \times 100\%$$

$$S_{C_xH_y} = \frac{\frac{x}{3} * F_{C_xH_y}}{F_{in, C_3H_8} - F_{out, C_3H_8}} \times 100\%$$

$$Yield = X_{C_3H_8} \times S_{C_3H_6}$$



Scheme 1: Experimental setup of the fixed-bed reactor used for the catalytic measurements

Results and discussion

Structural implications of Fe-doped CeO₂ catalysts

X-ray diffractograms of the various Fe-doped ceria materials are shown in Figure 1. Upon calcination at 600°C, all the materials show that cerianite is the main crystalline phase (reference cerianite phase lines are also included). As compared to the

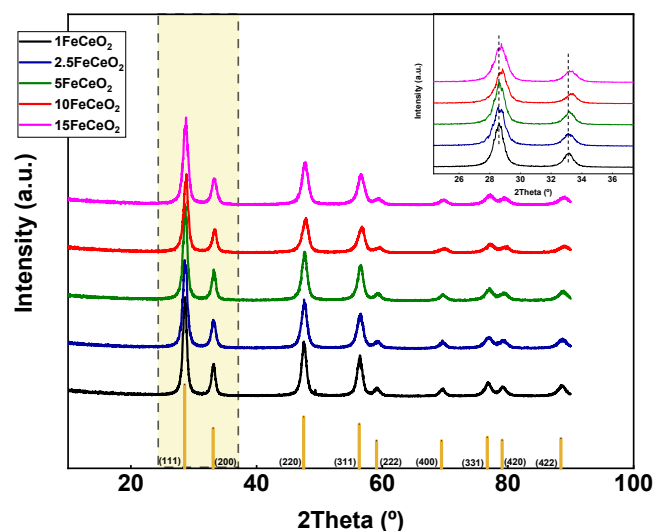


Figure 1: XRD patterns of catalytic materials synthesized with various Fe/Ce molar ratio. CeO₂ reference is shown also shown for comparison

reference cerianite, all diffraction peaks of the Fe-doped ceria samples shift to higher Bragg angles underscoring the formation of Fe-Ce solid solution, where Ce⁴⁺ cations are partially substituted by smaller Fe³⁺ ions inside cubic ceria structure²⁷. The small shift as well as observed broadening of the diffraction peaks indicate also possible changes of the crystallite sizes of cubic CeO₂; however, the average crystallite size of cubic CeO₂ as estimated from the corresponding (111) diffraction peak by means of the Debye-Scherrer equation (See Supporting Information, Table S1) appears to be within the 8-12nm without a monotonic behaviour across different samples. In addition, this type of partial substitution of Ce ions has the potential to result in different local environments of the oxygen atoms such as oxygen from the main ceria lattice phase, oxygen surrounded by Ce/Fe cations (Ce-rich) and/or oxygen surrounded by Fe/Ce cations (Fe-rich)³⁶. The diverse nature of oxygen atoms and/or vacancies created within the surface of CeO₂ have been highlighted as important active sites for propane activation. It is worth mentioning here that crystalline hematite (α -Fe₂O₃) phase was not detected by XRD for any of the samples tested indicating a good dispersion of Fe in the ceria lattice. The possibility of very small α -Fe₂O₃ crystals that lie below the detection limit of the XRD cannot be excluded.

Catalytic evaluation

Initial Screening of xFeCeO₂ catalysts

In Figure 2a, we present the catalytic evaluation screening, as referred to propane conversion and olefin selectivity for all catalysts synthesized. The data reported in Figure 2 pertain to initial reaction conditions, 20ml/min total flow (w/F=0.6 g.s/cc) and constant temperature at 550°C. The data collected for commercial CeO₂, Fe₂O₃ as well as their physical mixture (Fe₂O₃/CeO₂ = 1:20 molar ratio) are also included for comparison. The commercial CeO₂ shows very low conversion, less than 5%, with propylene selectivity to reach around 40%. Fe₂O₃ shows slightly higher propane conversion while the propylene selectivity decreased dramatically due to the formation of carbon oxides as discussed later. A physical

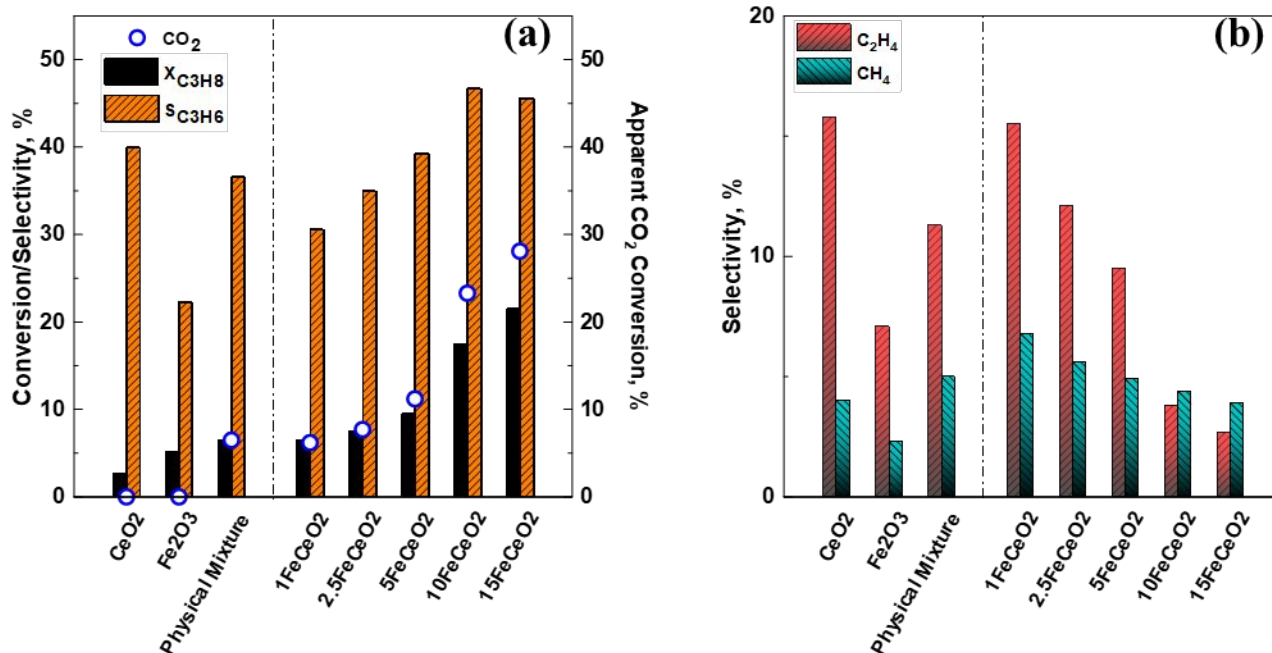
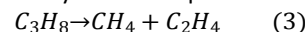


Figure 2: (a) Propane and apparent CO₂ conversion as well as propylene selectivity and (b) selectivity to ethylene and methane of all synthesized catalysts. Data pertain to initial reaction conditions, 20ml/min total flow (w/F=0.6 g.s/cc) and constant temperature at 550°C.

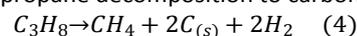
mixture of the commercial CeO₂ and Fe₂O₃ resulted to almost double propane conversion (as compared to pure CeO₂) with the propylene selectivity to reach almost that of pure CeO₂. Although moderate temperature treatment (close to the reaction temperature, i.e. 550°C) of CeO₂ and Fe₂O₃ physical mixtures does not alter significantly the local structure of the individual oxides, it is reported that the reducibility and overall redox properties can be enhanced just through their physical contact³⁷. The incorporation of small amount of Fe (1FeCeO₂) in ceria structure as dopant leads to a significant increase in propane conversion while propylene selectivity slightly decreases as compared to pure CeO₂. Upon increasing of Fe content, a monotonic increasing trend in propane conversion was observed from 6.5% (1FeCeO₂) to 21.5% (15FeCeO₂). Interestingly, although the conversion increases, the same behaviour was observed for the selectivity towards the propylene, reaching a maximum of around 47% for the 10FeCeO₂ catalyst. The increase in propane conversion can be partially associated with the increase in surface area of the catalysts (see Table S1 of the supporting information). A maximum in propylene selectivity and propane conversion is achieved between 10FeCeO₂ and 15FeCeO₂ with the initial yield to reach ~10% for the 15FeCeO₂ catalyst at 550°C. Besides the slightly higher surface area, the results suggest that there is a promotional effect of Fe as dopant on the activity of C-H bond activation. This effect can be associated to relative changes induced in active species with different local oxygen environments. As Fan et al.³⁶ demonstrated in a recent DFT study of ethylbenzene ODH on ZrCeO_x, the C-H bond activation is positively correlated with charge transferred from adsorbed hydrocarbon species to catalyst surface. It is likely that higher Fe concentration benefits the formation of Fe-rich oxygen sites rather than Ce-rich or Ce lattice oxygen species, which in turn results in advantages from two different aspects: lowering of reaction activation energy barrier and favoring the formation of oxygen vacancies in ceria surface lattice. The former has the

potential to improve the catalytic activity, i.e. propane conversion, while the latter is observed to be closely associated with propylene selectivity, which is discussed in later section.

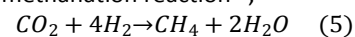
In Figure 2b, the selectivity patterns to methane and ethylene are also shown. A monotonic decrease in the formation of methane and ethylene is clear as more Fe is incorporated in the catalyst structure. The most straightforward propane conversion pathway towards ethylene and methane is the catalytic cracking which stoichiometrically results in 1:1 molar ratio between these hydrocarbon products:



In low Fe content catalysts, the molar ratio of methane-to-ethylene is very close to 1 (See Figure S2 of Supplementary Information), up to 5FeCeO₂ indicating that selectivity loss is associated to propane cracking. On the other hand, methane-to-ethylene molar ratio increased by two-fold over 10FeCeO₂ and 15FeCeO₂, which suggests that additional reaction pathways may exist that lead to the formation of excess methane. Among the possible reaction pathways towards methane, the propane decomposition to carbon deposits,



is likely to occur at the temperature range of our experiments while the CO₂ methanation reaction³⁸,



cannot be excluded. The former reaction is expected to severely affect the stability of these catalysts and will be discussed in more detail at a later section. However, the total selectivity of methane and ethylene decrease significantly at high Fe content indicating that these pathways do not dominate the catalytic performance under these reaction conditions.

The improved catalytic performance of the 10FeCeO₂ and 15FeCeO₂ catalysts is associated with the lower amount of other hydrocarbon by-products present under our reaction conditions. Considering that the overall carbon balance as calculated based on the total carbon flow of all gaseous reactants/products is usually above 98-99%, the rest carbon

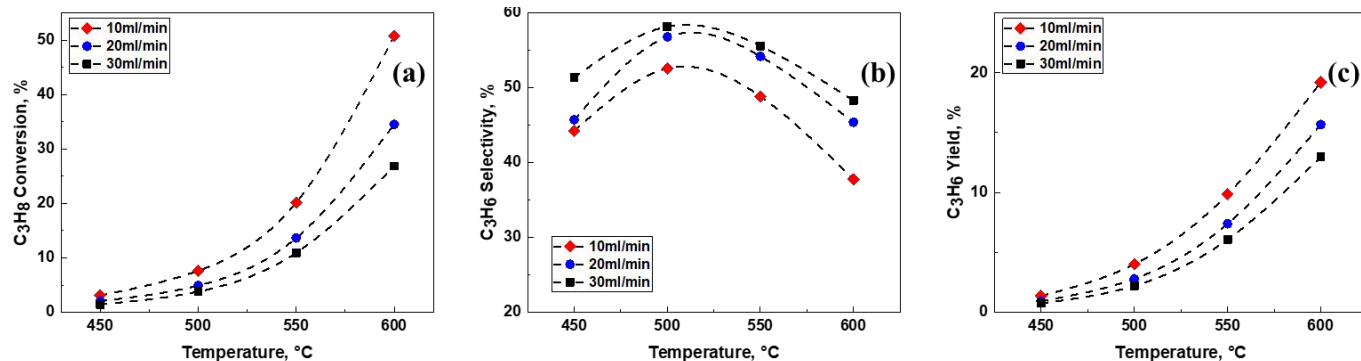


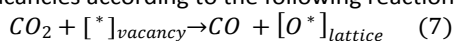
Figure 2: Effect of temperature as well as residence time on (a) propane conversion, (b) propylene selectivity and (c) propylene yield, of the most selective, 10FeCeO₂, catalyst. Data pertain to initial reaction conditions

flow pertains to carbon oxides, CO and CO₂. It must be highlighted here that the majority of carbon oxides pertains to CO that is also consistent with previous reports^{23, 25, 39}.

Although CO₂ formation from deep oxidation is plausible, CO₂ readily reacts over the catalytic surface under our reaction conditions as shown also in Figure 2a. It is evident that the addition of Fe in the ceria shows a monotonic increase in the apparent CO₂ conversion that resembles the propane conversion behavior. The maximum CO₂ conversion (~30%) was observed for the 15FeCeO₂ catalyst. In carbon dioxide assisted alkane oxidative dehydrogenation reaction it is well recognized that CO₂ participates mainly in the RWGS reaction which in turns favours propane conversion as discussed earlier. The catalytic behavior presented here for the Fe-doped catalysts appears to be consistent with the aforementioned reaction scheme, but the difference in product selectivity across different catalysts underscores the complexity of the reaction network that exists. In addition, recent report³⁸ highlight also the possibility of CO₂ participation in methanation (reaction 5) as well as in propane dry reforming reaction (reaction 6).



Very recently, the concept of CO₂ dissociation over reduced metal oxides was also introduced in light of reoxidizing surface oxygen vacancies according to the following reaction⁴⁰.



However, it is hard to clearly distinguish the actual selectivity to CO and/or CO₂ due to the uncertainty of relative contribution of CO production from either propane combustion, reverse water gas shift reaction, dry reforming, reverse Boudouard reaction or CO₂ splitting. Future experimental endeavours towards the establishment of kinetic and mechanistic understanding can shed light on the actual role of CO₂ on the activity, stability and/or deactivation of the catalyst reported herein.

Effect of temperature and residence time on catalytic activity

Next, we evaluate the effect of temperature as well as residence time on the catalytic performance of the most selective, 10FeCeO₂, catalyst. Specifically, we assess the catalyst activity in the 450°C–600°C temperature range while we also varied the total flow of reaction mixture within the 10–30 ml/min range. Figure 3 compares relevant results for the propane conversion as well as propylene selectivity and yield. The selectivity to other products is also shown in Figure S3 of the Supporting

Information. Upon increasing temperature and/or reducing residence time (W/F), the propane conversion increases significantly reaching a maximum of 52% at 600°C and 0.33 g_{cat}⁻¹h/L. The selectivity to propylene is monotonically reduced upon increasing the residence time which is associated with consecutive paraffin/olefin oxidation to CO_x as shown also in Figure S3. Propylene selectivity reaches a maximum upon increasing temperature around 500–550°C while a decrease is observed at higher temperature. The decrease in selectivity at high temperature is attributed to combustion to CO_x, thermal cracking of propane as well as consecutive oxidation of propylene by either catalyst surface oxygen species or carbon dioxide⁴¹. Thermodynamic analysis of standard Gibbs free energy change of light alkanes and olefins cracking shows that spontaneity of olefin cracking outweigh alkane cracking, especially at high temperatures⁴². This is also consistent with our experimental results presented in supporting information that show a monotonic increase in selectivity to ethylene and methane, the major products of C₃ cracking. It is very important here to underscore that the propane cracking and overall catalyst deactivation can be also associated with the presence of acidic sites on the catalyst surface. In oxygen assisted alkane ODH it has been shown that the strength of Lewis acidity of the cation sites of the catalyst besides selective C–H activation leads also to non-selective activation and combustion. However, study on Fe-doped CeO₂ catalysts with similar Fe loading has shown that even though the incorporation of Fe increases the amount of Brønsted and Lewis acids (as compared to the pure CeO₂ support), their intrinsic strength is relatively low as revealed from in-situ IR coupled with NH₃-TPD⁴³. Under similar reaction conditions, Nijhuis et al. reported the formation of coke deposits at different positions of the catalyst bed as revealed by in-situ Raman and thermogravimetric studies. They found that significantly less coke was observed at the top catalyst layers than the middle and bottom parts of the catalyst bed⁴⁴. Since 550°C show promising propylene selectivity, next we evaluate the stability of all catalysts synthesized with time on stream.

Effect of C₃H₈/CO₂ in the feed on propane ODH

The effect of the C₃H₈/CO₂ in the feed on the catalytic performance of the most selective catalyst identified, i.e. 10%FeCeO₂, was studied under 550°C and total flow of 20 ml/min. Relevant results concerning propane conversion and

propylene selectivity are summarized in Figure 4. Our data show that higher partial pressure of CO₂ in the feed mixture results in slight decrease in conversion for feeds rich in propane and almost no change for low propane initial concentration. In all

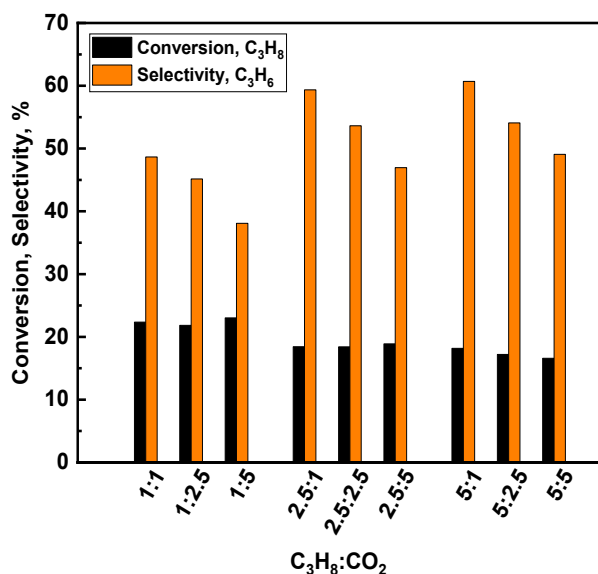


Figure 4: Effect of propane and/or carbon dioxide partial pressure on the catalytic performance. Catalyst: 10FeCe600. Reaction conditions: 550°C, 20mL total flow, 200mg catalyst loading.

cases, a marked decrease in propylene selectivity was observed. The highest propylene selectivity exceeded 60% for 5:1 C₃H₈/CO₂ ratio in the reaction feed while propane conversion was maintained at ~18% resulting in a maximum of ~11% propylene yield. On equimolar feeds, the propylene selectivity remains the same while propane conversion increases in the presence of dilute feeds (1:1). These results in conjunction with the preceding discussion suggest that the observed negative effect of CO₂ on propylene selectivity could be attributed to the promotion in propane dry reforming pathway.

Time-on-stream catalytic performance and deactivation

Figure 5(a-c) displays the propane conversion and selectivity of major products on three Fe-doped CeO₂ samples with time-on-stream (stability performance of all the rest catalysts is listed at the Supporting Information, Figure S4). The stability of catalysts was tested for 20-24hr time-on-stream. We observe that the

selectivity to propylene appears to be stable for most of the catalytic materials tested. With a closer look at the Fe-doped catalysts with large Fe/Ce ratio, an increase in propylene selectivity is observed within the first 2-4 hours of reaction and then remained stable. For the 10FeCeO₂ catalyst, this increase was almost 10% and was accompanied by a gradual decrease in propane conversion from 17.5% to 14%. Similar behaviour was observed for the 15FeCeO₂ catalyst. Contrary, for low Fe concentration catalysts, the propane conversion is more stable with time-on-stream; the best stability performance was observed for the 5FeCeO₂ catalyst. More specifically, the conversion for the 1, 2.5 and 5FeCeO₂ catalysts was found to be stable up to 6, 10 and 15 hours respectively while for the rest catalysts a monotonic decrease is observed.

It is worth mentioning here that for the low Fe concentration catalysts, the gradual decrease of propane conversion at very long time-on-stream is accompanied by a simultaneous increase in the selectivity of ethylene and methane. This result suggests that the observed deactivation observed is also associated probably with consecutive paraffin and/or olefin cracking that can lead to lighter hydrocarbons and/or coke. On the other hand, even though a monotonic decrease in propane conversion was observed for the catalysts with large Fe/Ce ratio, no significant change was noticed in methane and ethylene selectivity. These results underscore that between low and high Fe/Ce catalysts, different deactivation mechanisms may exist that directly affect the stability in their catalytic performance. In order to investigate the effect of CO₂ on the stability of our catalysts, experiments were also conducted in the absence of CO₂ in the reaction feed for the 10FeCeO₂ catalysts and relevant results shown in Figure S5 of the supporting information. By comparing relevant catalytic results under identical reaction conditions, we observe an increase of the initial propane conversion when no CO₂ was present in the reaction feed while initial propylene selectivity was almost the same. With time-on-stream, there is a very rapid deactivation of the 10FeCeO₂ catalyst as can be clearly seen from the monotonic and rapid drop in propane conversion. The rapid deactivation is accompanied by the simultaneous monotonic increase in the selectivity of ethylene indicating the presence of propane cracking among the primary pathways. It appears that the presence of CO₂ in the feed helps improving the stability performance of the catalysts probably due to the reoxidation of surface active sites and/or by in-situ removing coke deposits

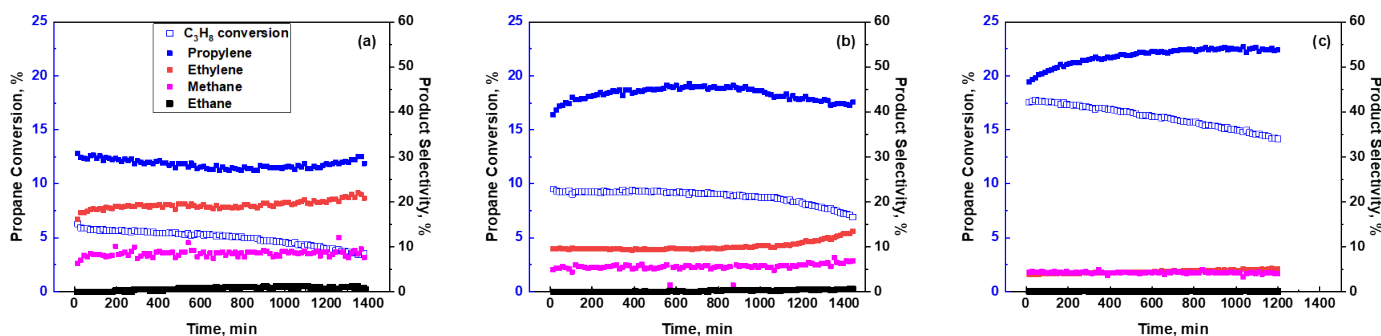


Figure 5: Time-on-stream catalytic performance of (a) 1FeCeO₂, (b) 5FeCeO₂ and (c) 10FeCeO₂ catalyst. Data pertain to 20ml/min total flow (w/F=0.6 g.s/cc) and constant temperature at 550°C.

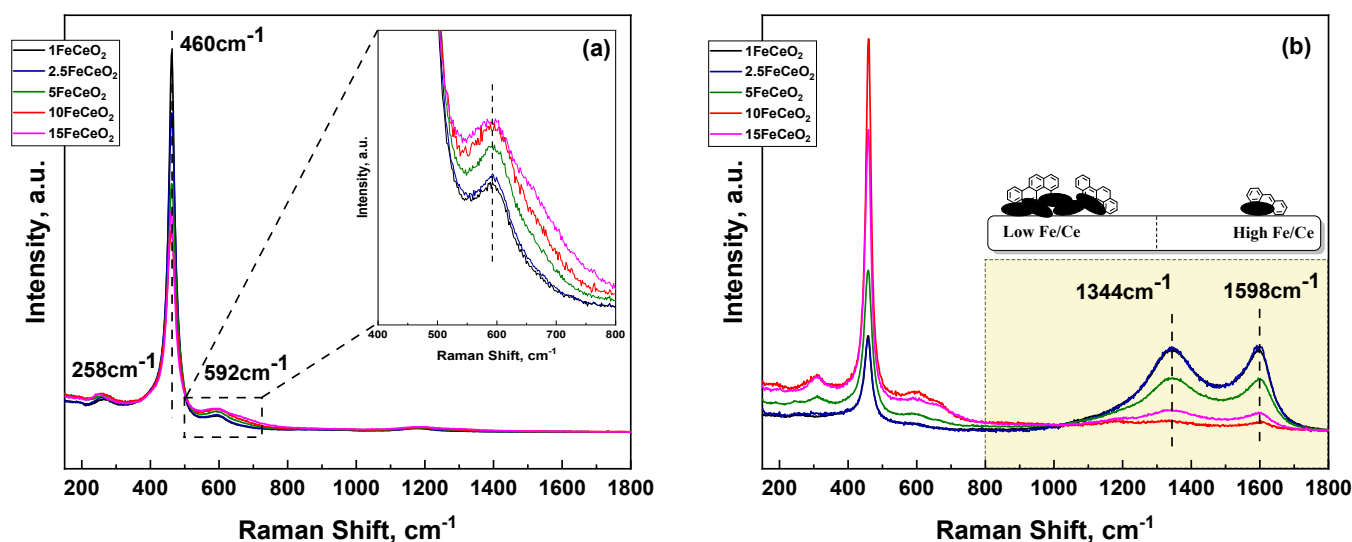


Figure 6: Raman spectra of (a) fresh catalysts (inset show the 400-800 cm^{-1} enlarged) and (b) spent catalysts.

from the surface via the reverse Boudouard reaction. We believe that the initial improvement of propane conversion can be associated with the promotion of propane adsorption on all available and accessible active sites. This hypothesis is also in agreement with a recent study on FeNi/CeO₂ systems^{25, 45} where the competitive adsorption between propane and CO₂ was highlighted among the key-factors controlling catalyst productivity.

To further investigate the reasons behind the observed deactivation, thorough characterization of the fresh and post reaction catalysts has been performed via Raman spectroscopy. Raman spectroscopy is a powerful tool for the structural characterization of metal oxides⁴⁶⁻⁴⁷. Figure 6a shows the Raman spectra of the fresh catalysts after calcination. The spectral envelope in the 200-800 cm^{-1} range displays a very strong band located at 460 cm^{-1} which is associated with the F_{2g} vibrational mode of CeO₂⁴⁸. Upon increasing of Fe, a very small shift was observed to lower wavenumbers that is ascribed to the gradual doping of CeO₂ lattice with Fe and is consistent with the XRD results discussed at an earlier section. A closer look shows a monotonic increase in intensity of D band (Figure 6a-inset) located at 592 cm^{-1} which is associated with the presence of substoichiometric CeO_{2-x} units underscoring an increase in oxygen vacancies⁴⁹. The relative intensity ratio of 592 cm^{-1} and 460 cm^{-1} , I_{592}/I_{460} , has been routinely used in the open literatures⁵⁰⁻⁵² as an indicator of the presence of oxygen vacancies in CeO₂ based materials. The I_{592}/I_{460} is shown in the Supporting Information, Figure S6. We observe that the I_{592}/I_{460} reaches a maximum at high Fe/Ce catalysts. This trend resembles the increase in propylene selectivity thus suggesting the possible participation of oxygen deficient site in the selective dehydrogenation pathway. On the other hand, post-reaction Raman characterization shown in Figure 6b, show the presence of two broad and intense peaks located at 1344 cm^{-1} and 1598 cm^{-1} which are associated with the G and D bands of carbon deposits^{7, 53-54}. At low Fe/Ce, coke is favoured while at high Fe/Ce catalysts coke is minimal. This result suggests that the gradual deactivation of low Fe/Ce catalysts is due to the

formation of carbon deposits on the surface which is also consistent with the increased selectivity towards cracking products as discussed earlier. However, one cannot exclude possible reactivity loss due to rapid reduction of available active sites under these reaction conditions. It has been shown that a small amount of Fe incorporation in CeO₂ lowers the reduction temperature of the main surface oxygen sites from ~520°C to the range of 370-400°C indicating a weakening of surface Ce-O bonds that leads to an enhanced oxygen mobility. Although H₂-TPR/O₂-TPO experimentation has shown to be a valuable tool

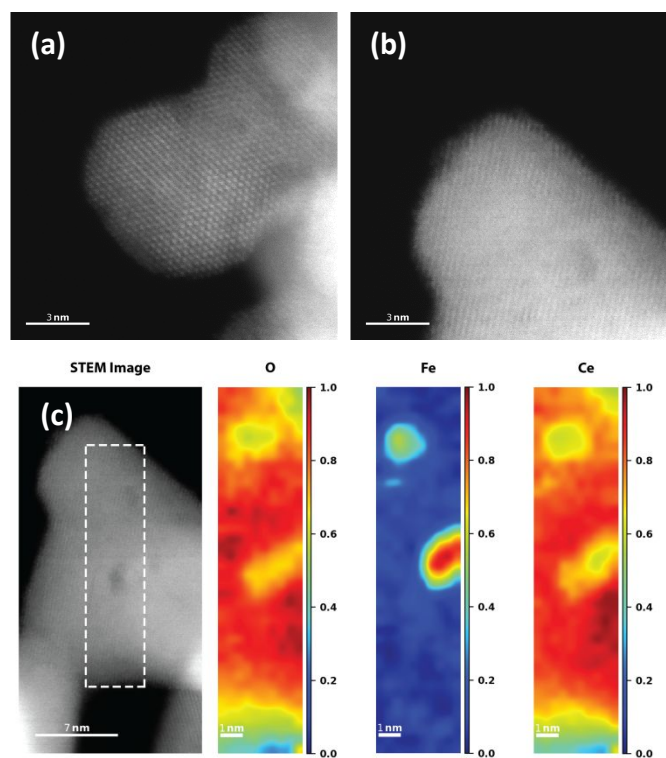


Figure 7: High resolution STEM images of the 10%FeCeO₂ catalyst particles before (a) and after (b) reaction. (c) The dashed box indicates the element mapping area and its corresponding oxygen, iron, and cerium distribution maps.

towards understanding the redox properties of Fe-doped CeO₂ catalysts^{43, 55-56}, future research endeavors towards an in-depth investigation of cyclic H₂-TPR and CO₂-TPO experiment can provide insights into the product distribution and contribution of CO₂ as an oxidizing agent. Coupling these measurements with advanced Operando spectroscopic techniques such as Raman and IR can disentangle the contribution of individual active sites to the overall performance while providing at the same time molecular level information on catalyst deactivation.

In addition, ex-situ XPS was applied to investigate the chemical states of highly ordered carbon nanostructures deposited over fresh and spent iron-cerium oxides. Symmetrical sp³ peak (284.6~284.8eV) and asymmetrical sp² peak (284.2~284.3eV) was fitted to the C1s main feature for post-reaction catalysts⁵⁷. The detailed deconvolution is shown in the supporting information (Figure S7). An apparent increase was observed in C/O ratio for up to 5FeCeO₂ spent catalysts as opposed to fresh material, where the C/O basis was estimated within 20~30%. A major contribution of this carbon amount lies in the advent of sp² peak fitted on the basis of the invariant sp³ peak, revealing aromatic structure as primary chemical states of coke. As higher Fe-dopant concentration was reached, C/O ratio decreases together with sp² peak area percentage, observation that is consistent with our Raman data. Particularly, C/O ratio fell into the range of reference fresh material, which is a strong proof of minor carbon deposition after 24-hour ODH reaction. Although the suppressed formation of coke deposits appears to be associated with the higher propylene selectivity observed, the reasons behind the monotonic decrease in the conversion for the high Fe/Ce catalysts is still elusive.

In an effort to gain more insight into the observed catalytic behaviour of the 10FeCeO₂, samples before and after reaction were investigated using a scanning transmission electron microscope (STEM). Typical catalyst particles before and after reaction are shown in Figure 7(a-c). It is observed that the particle size before the reaction is less than 10 nm (consistent with XRD results) while the particle size after the reaction is in general larger than 15 nm. This result points to the decrease in specific surface area due to sintering as one possible reason behind the observed catalyst deactivation as seen from the conversion of propane in time-on-stream. In addition, element mapping was carried out for the after-reaction sample. As show in Figure 7c, iron is found in two localized areas in the mapped area. The result suggests that, besides CeO₂ sintering, iron also migrates to localized areas instead of keeping its initial solid solution form during the reaction indicating a significant change in morphology of the catalysts which can in turn affect the overall catalytic performance.

Conclusions

CO₂-assisted propane oxidative dehydrogenation reaction was tested over a series of Fe-doped cerium oxide catalysts with varied Fe/Ce ratio from 1% to 15%. It is demonstrated that both propane conversion and propylene selectivity were improved at higher Fe/Ce ratio, indicating that propane ODH pathway is favored over Fe-rich surfaces. Careful examination on reaction by-products revealed propane cracking and dry reforming as

two major side reactions in the reaction system. At high Fe/Ce ratio, cracking reactions appear to be minimized. In general, all catalysts exhibit comparably stable catalytic behavior for over 20 hours continuous catalytic test, with 5FeCeO₂ standing out as the most stable catalyst. Raman, XPS and STEM characterizations of post-reaction catalysts were performed in order to study possible reasons for xFeCeO₂ catalyst deactivation. Our characterization results unveiled that at low Fe/Ce ratio, carbon deposition and coke formation is the primary reason that hampers propane conversion while at high Fe/Ce ratio, the FeCeO₂ catalysts suffer from ceria crystal sintering and Fe migration to nano-size crystals.

Conflicts of interest

There are no conflicts to declare.

Acknowledgements

This material is based upon work supported in part by Rutgers, The State University of New Jersey, and the National Science Foundation Award #1751683. The authors would like to thank Prof. A. Neimark and Prof. T. Asefa for helping with the BET measurements and porosity analysis, Prof. P. Batson and Dr. Y. Yeh for the STEM images and Dr. W. Zheng for the XPS data.

Notes and references

- Gärtner, C. A.; van Veen, A. C.; Lercher, J. A., Oxidative Dehydrogenation of Ethane: Common Principles and Mechanistic Aspects. *ChemCatChem* **2013**, *5* (11), 3196-3217.
- Carrero, C. A.; Schloegl, R.; Wachs, I. E.; Schomaecker, R., Critical Literature Review of the Kinetics for the Oxidative Dehydrogenation of Propane over Well-Defined Supported Vanadium Oxide Catalysts. *ACS Catalysis* **2014**, *4* (10), 3357-3380.
- Cavani, F.; Ballarini, N.; Cericola, A., Oxidative dehydrogenation of ethane and propane: How far from commercial implementation? *Catalysis Today* **2007**, *127* (1-4), 113-131.
- Vora, B. V., Development of Dehydrogenation Catalysts and Processes. *Topics in Catalysis* **2012**, *55* (19-20), 1297-1308.
- Blay, V.; Epelde, E.; Miravalles, R.; Perea, L. A., Converting olefins to propene: Ethene to propene and olefin cracking. *Catalysis Reviews* **2018**, *60* (2), 278-335.
- Sun, L.; Chai, Y.; Dai, W.; Wu, G.; Guan, N.; Li, L., Oxidative dehydrogenation of propane over Pt-Sn/Si-beta catalysts: key role of Pt-Sn interaction. *Catalysis Science & Technology* **2018**, *8* (12), 3044-3051.
- Li, Q.; Sui, Z.; Zhou, X.; Zhu, Y.; Zhou, J.; Chen, D., Coke Formation on Pt-Sn/Al₂O₃ Catalyst in Propane Dehydrogenation: Coke Characterization and Kinetic Study. *Topics in Catalysis* **2011**, *54* (13-15), 888-896.
- Kawi, S.; Kathiraser, Y., CO₂ as an oxidant for high-temperature reactions. *Front Energy Res* **2015**.
- Botavina, M. A.; Agafonov, Y. A.; Gaidai, N. A.; Groppo, E.; Cortés Corberán, V.; Lapidus, A. L.; Martra, G., Towards efficient catalysts for the oxidative dehydrogenation of propane in the presence of CO₂: Cr/SiO₂ systems prepared by direct hydrothermal synthesis. *Catalysis Science & Technology* **2016**, *6* (3), 840-850.
- Takehira, K.; Ohishi, Y.; Shishido, T.; Kawabata, T.; Takaki, K.; Zhang, Q.; Wang, Y., Behavior of active sites on Cr-MCM-41 catalysts

- during the dehydrogenation of propane with CO₂. *Journal of Catalysis* **2004**, *224* (2), 404-416.
11. Yun, D.; Baek, J.; Choi, Y.; Kim, W.; Lee, H. J.; Yi, J., Promotional Effect of Ni on a CrO_xCatalyst Supported on Silica in the Oxidative Dehydrogenation of Propane with CO₂. *ChemCatChem* **2012**, *4* (12), 1952-1959.
12. Baek, J.; Yun, H. J.; Yun, D.; Choi, Y.; Yi, J., Preparation of Highly Dispersed Chromium Oxide Catalysts Supported on Mesoporous Silica for the Oxidative Dehydrogenation of Propane Using CO₂: Insight into the Nature of Catalytically Active Chromium Sites. *ACS Catalysis* **2012**, *2* (9), 1893-1903.
13. Michorczyk, P.; Pietrzyk, P.; Ogonowski, J., Preparation and characterization of SBA-1-supported chromium oxide catalysts for CO₂ assisted dehydrogenation of propane. *Microporous and Mesoporous Materials* **2012**, *161*, 56-66.
14. Michorczyk, P.; Ogonowski, J.; Zeńczak, K., Activity of chromium oxide deposited on different silica supports in the dehydrogenation of propane with CO₂ – A comparative study. *Journal of Molecular Catalysis A: Chemical* **2011**, *349* (1-2), 1-12.
15. Burri, A.; Hasib, M. A.; Mo, Y.-H.; Reddy, B. M.; Park, S.-E., An Efficient Cr-TUD-1 Catalyst for Oxidative Dehydrogenation of Propane to Propylene with CO₂ as Soft Oxidant. *Catalysis Letters* **2017**, *148* (2), 576-585.
16. Botavina, M.; Barzan, C.; Piovano, A.; Braglia, L.; Agostini, G.; Martra, G.; Groppo, E., Insights into Cr/SiO₂ catalysts during dehydrogenation of propane: an operando XAS investigation. *Catalysis Science & Technology* **2017**, *7* (8), 1690-1700.
17. Michorczyk, P.; Ogonowski, J.; Niemczyk, M., Investigation of catalytic activity of CrSBA-1 materials obtained by direct method in the dehydrogenation of propane with CO₂. *Applied Catalysis A: General* **2010**, *374* (1-2), 142-149.
18. Zhu, Q.; Takiguchi, M.; Setoyama, T.; Yokoi, T.; Kondo, J. N.; Tatsumi, T., Oxidative Dehydrogenation of Propane with CO₂ Over Cr/H[B]MFI Catalysts. *Catalysis Letters* **2011**, *141*, 670-677.
19. Agafonov, Y. A.; Gaidai, N. A.; Lapidus, A. L., Influence of the preparation conditions for catalysts CrO_x/SiO₂ on their efficiency on propane dehydrogenation in the presence of CO₂. *Russian Chemical Bulletin* **2014**, *63*, 381-388.
20. Zhang, F.; Wu, R.; Yue, Y.; Yang, W.; Gu, S.; Miao, C.; Hua, W.; Gao, Z., Chromium oxide supported on ZSM-5 as a novel efficient catalyst for dehydrogenation of propane with CO₂. *Microporous and Mesoporous Materials* **2011**, *145* (1-3), 194-199.
21. Yan, B.; Yao, S.; Kattel, S.; Wu, Q.; Xie, Z.; Gomez, E.; Liu, P.; Su, D.; Chen, J. G., Active sites for tandem reactions of CO₂ reduction and ethane dehydrogenation. *Proc Natl Acad Sci U S A* **2018**, *115* (33), 8278-8283.
22. Gomez, E.; Yan, B.; Kattel, S.; Chen, J. G., Carbon dioxide reduction in tandem with light-alkane dehydrogenation. *Nature Reviews Chemistry* **2019**, *3*, 638-649.
23. Gomez, E.; Kattel, S.; Yan, B.; Yao, S.; Liu, P.; Chen, J. G., Combining CO₂ reduction with propane oxidative dehydrogenation over bimetallic catalysts. *Nat Commun* **2018**, *9* (1), 1398.
24. Yan, B.; Yang, X.; Yao, S.; Wan, J.; Myint, M.; Gomez, E.; Xie, Z.; Kattel, S.; Xu, W.; Chen, J. G., Dry Reforming of Ethane and Butane with CO₂ over PtNi/CeO₂ Bimetallic Catalysts. *ACS Catalysis* **2016**, *6* (11), 7283-7292.
25. Gomez, E.; Xie, Z. H.; Chen, J. G. G., The effects of bimetallic interactions for CO₂-assisted oxidative dehydrogenation and dry reforming of propane. *Aiche Journal* **2019**, *65* (8).
26. Yan, B. H.; Yao, S. Y.; Chen, J. G. G., Effect of Oxide Support on Catalytic Performance of FeNi-based Catalysts for CO₂-assisted Oxidative Dehydrogenation of Ethane. *Chemcatchem* **2020**, *12* (2), 494-503.
27. Campbell, C. T.; Peden, C. H. F., Oxygen Vacancies and Catalysis on Ceria Surfaces. *SCIENCE* **2005**, *309* (5735), 713-714.
28. Perez-Alonso, F. J.; Lopez Granados, M.; Ojeda, M.; Terreros, P.; Rojas, S.; Herranz, T.; Fierro, J. L. G., Chemical Structures of Coprecipitated Fe-Ce Mixed Oxides. *Chem. Mater.* **2005**, *17*, 2329-2339.
29. Michorczyk, P.; Kustrowski, P.; Chmielarz, L.; Ogonowski, J., Influence of redox properties on the activity of iron oxide catalysts in dehydrogenation of propane with CO₂. *React. Kinet. Catal. Lett* **2004**, *82*, 121-130.
30. Kowalska-Kuś, J.; Held, A.; Nowińska, K., Oxydehydrogenation of C₂-C₄hydrocarbons over Fe-ZSM-5 zeolites with N₂O as an oxidant. *Catal. Sci. Technol.* **2013**, *3* (2), 508-518.
31. Scheffe, J. R.; Steinfeld, A., Oxygen exchange materials for solar thermochemical splitting of H₂O and CO₂: a review. *Materials Today* **2014**, *17* (7), 341-348.
32. Galvita, V. V.; Poelman, H.; Bliznuk, V.; Detavernier, C.; Marin, G. B., CeO₂-Modified Fe₂O₃ for CO₂ Utilization via Chemical Looping. *Industrial & Engineering Chemistry Research* **2013**, *52* (25), 8416-8426.
33. Sahoo, S. K.; Mohapatra, M.; Pandey, B.; Verma, H. C.; Das, R. P.; Anand, S., Preparation and characterization of α-Fe₂O₃-CeO₂ composite. *Materials Characterization* **2009**, *60* (5), 425-431.
34. Li, K.; Wang, H.; Wei, Y.; Yan, D., Direct conversion of methane to synthesis gas using lattice oxygen of CeO₂-Fe₂O₃ complex oxides. *Chemical Engineering Journal* **2010**, *156* (3), 512-518.
35. Rossi, A. F.; Amaral-Silva, N.; Martins, R. C.; Quinta-Ferreira, R. M., Heterogeneous Fenton using ceria based catalysts: effects of the calcination temperature in the process efficiency. *Applied Catalysis B: Environmental* **2012**, *111-112*, 254-263.
36. Fan, H.-X.; Feng, J.; Li, W.-Y., Promotional effect of oxygen storage capacity on oxy-dehydrogenation of ethylbenzene with CO₂ over κ-Ce₂Zr₂O₈(111). *Applied Surface Science* **2019**, *486*, 411-419.
37. Gu, Z. H.; Li, K. Z.; Qing, S.; Zhu, X.; Wei, Y. G.; Li, Y. T.; Wang, H., Enhanced reducibility and redox stability of Fe₂O₃ in the presence of CeO₂ nanoparticles. *Rsc Advances* **2014**, *4* (88), 47191-47199.
38. Cárdenas-Arenas, A.; Quindimil, A.; Davó-Quifonero, A.; Bailón-García, E.; Lozano-Castelló, D.; De-La-Torre, U.; Pereda-Ayo, B.; González-Marcos, J. A.; González-Velasco, J. R.; Bueno-López, A., Isotopic and in situ DRIFTS study of the CO₂ methanation mechanism using Ni/CeO₂ and Ni/Al₂O₃ catalysts. *Applied Catalysis B: Environmental* **2020**, *265*.
39. Atanga, M. A.; Rezaei, F.; Jawad, A.; Fitch, M.; Rownaghi, A. A., Oxidative dehydrogenation of propane to propylene with carbon dioxide. *Appl Catal B-Environ* **2018**, *220*, 429-445.
40. Nowicka, E.; Reece, C.; Althahban, S. M.; Mohammed, K. M. H.; Kondrat, S. A.; Morgan, D. J.; He, Q.; Willock, D. J.; Golunski, S.; Kiely, C. J.; Hutchings, G. J., Elucidating the Role of CO₂ in the Soft Oxidative Dehydrogenation of Propane over Ceria-Based Catalysts. *ACS Catalysis* **2018**, *8* (4), 3454-3468.
41. Xie, Z.; Ren, Y.; Li, J.; Zhao, Z.; Fan, X.; Liu, B.; Song, W.; Kong, L.; Xiao, X.; Liu, J.; Jiang, G., Facile in situ synthesis of highly dispersed chromium oxide incorporated into mesoporous ZrO₂ for the dehydrogenation of propane with CO₂. *Journal of Catalysis* **2019**, *372*, 206-216.
42. Du, X.; Yao, B.; Gonzalez-Cortes, S.; Kuznetsov, V. L.; AlMegren, H.; Xiao, T.; Edwards, P. P., Catalytic dehydrogenation of propane by carbon dioxide: a medium-temperature thermochemical process for carbon dioxide utilisation. *Faraday Discuss* **2015**, *183*, 161-76.
43. Peng, Y.; Yu, W. W.; Su, W. K.; Huang, X.; Li, J. H., An experimental and DFT study of the adsorption and oxidation of NH₃ on a CeO₂ catalyst modified by Fe, Mn, La and Y. *Catal Today* **2015**, *242*, 300-307.

44. Nijhuis, T. A.; Tinnemans, S. J.; Visser, T.; Weckhuysen, B. M., Towards real-time spectroscopic process control for the dehydrogenation of propane over supported chromium oxide catalysts. *Chemical Engineering Science* **2004**, *59* (22-23), 5487-5492.
45. Gomez, E.; Kattel, S.; Yan, B. H.; Yao, S. Y.; Liu, P.; Chen, J. G. G., Combining CO₂ reduction with propane oxidative dehydrogenation over bimetallic catalysts. *Nature Communications* **2018**, *9*.
46. Tsilomelekis, G.; Boghosian, S., Structural and vibrational properties of molybdena catalysts supported on alumina and zirconia studied by in situ Raman and FTIR spectroscopies combined with ¹⁸O/¹⁶O isotopic substitution. *Catalysis Today* **2010**, *158* (1-2), 146-155.
47. Tribalis, A.; Panagiotou, G. D.; Tsilomelekis, G.; Kalamounias, A. G.; Bourikas, K.; Kordulis, C.; Boghosian, S.; Lycourghiotis, A., Temperature-Dependent Evolution of the Molecular Configuration of Oxo-Tungsten(VI) Species Deposited on the Surface of Titania. *The Journal of Physical Chemistry C* **2014**, *118* (21), 11319-11332.
48. Penkala, B.; Aubert, D.; Kaper, H.; Tardivat, C.; Conder, K.; Paulus, W., The role of lattice oxygen in CO oxidation over Ce₁₈O₂-based catalysts revealed under operando conditions. *Catalysis Science & Technology* **2015**, *5* (10), 4839-4848.
49. Huang, W.; Gao, Y., Morphology-dependent surface chemistry and catalysis of CeO₂ nanocrystals. *Catal. Sci. Technol.* **2014**, *4* (11), 3772-3784.
50. Wu, Z.; Rondinone, A. J.; Ivanov, I. N.; Overbury, S. H., Structure of Vanadium Oxide Supported on Ceria by Multiwavelength Raman Spectroscopy. *The Journal of Physical Chemistry C* **2011**, *115* (51), 25368-25378.
51. Luo, M.-F.; Yan, Z.-L.; Jin, L.-Y.; He, M., Raman Spectroscopic Study on the Structure in the Surface and the Bulk Shell of CexPr1-xO_{2-δ} Mixed Oxides. *J. Phys. Chem. B* **2006**, *110*, 13068-13071.
52. Ridwan, M.; Tamarany, R.; Han, J.; Nam, S. W.; Ham, H. C.; Kim, J. Y.; Choi, S. H.; Jang, S. C.; Yoon, C. W., Atomically dispersed Cu on Ce_{1-x}RE_xO_{2-δ} nanocubes (RE = La and Pr) for water gas shift: influence of OSC on catalysis. *RSC Advances* **2015**, *5* (109), 89478-89481.
53. An, H.; Zhang, F.; Guan, Z.; Liu, X.; Fan, F.; Li, C., Investigating the Coke Formation Mechanism of H-ZSM-5 during Methanol Dehydration Using Operando UV-Raman Spectroscopy. *ACS Catalysis* **2018**, *8* (10), 9207-9215.
54. Pocsik, I.; Hundhausen, M.; Koos, M.; Ley, L., Origin of the D peak in the Raman spectrum of microcrystalline graphite. *Journal of Non-Crystalline Solids* **1998**, *227-230*, 1083-1086.
55. Li, K. Z.; Haneda, M.; Ning, P. H.; Wang, H.; Ozawa, M., Microstructure and oxygen evolution of Fe-Ce mixed oxides by redox treatment. *Applied Surface Science* **2014**, *289*, 378-383.
56. Zhang, Z. L.; Han, D.; Wei, S. J.; Zhang, Y. X., Determination of active site densities and mechanisms for soot combustion with O₂ on Fe-doped CeO₂ mixed oxides. *J Catal* **2010**, *276* (1), 16-23.
57. Blume, R.; Rosenthal, D.; Tessonier, J.-P.; Li, H.; Knop-Gericke, A.; Schlögl, R., Characterizing Graphitic Carbon with X-ray Photoelectron Spectroscopy: A Step-by-Step Approach. *ChemCatChem* **2015**, *7* (18), 2871-2881.



Page 11 of Catalysis Science & Technology

